Inorg. Chem. **2007**, *46*, 1090–1099

Neutron Diffraction and Theoretical DFT Studies of Two Dimensional Molecular-Based Magnet $K_2[Mn(H_2O)_2]_3[Mo(CN)_7]_2 \cdot 6H_2O$

Béatrice Gillon,*,† Antoine Goujon,† Stéphanie Willemin,‡ Joulia Larionova,*,‡ Cédric Desplanches,§,£ Eliseo Ruiz,*,§ Gilles André,† John A. Stride,†,|| and Christian Guérin‡

Laboratoire Léon Brillouin, CEA/CNRS, UMR0012, Centre d'Etudes de Saclay, 91191, Gif sur Yvette, France, Laboratoire de Chimie Moléculaire et Organisation du Solide, UMR 5637, Université Montpellier II, Place E. Bataillon, 34095 Montpellier cedex 5, France, Departament de Química Inorgànica, and Centre Especial de Recerca en Química Teòrica (CeRQT), Universitat de Barcelona, Diagonal 647, 08028 Barcelona, Spain

Received June 26, 2006

Exchange mechanisms and magnetic structure in the two-dimensional cyano-bridged molecule-based magnet $K_2[Mn(H_2O)_2]_3[Mo(CN)_7]_2 \cdot 6H_2O$ have been investigated by a combination of neutron diffraction studies on both single crystal and powder samples and theoretical DFT calculations. The experimental spin density has been deduced from a new refinement of previously obtained polarized neutron diffraction (PND) data which was collected in the ordered magnetic state at 4 K under a saturation field of 3 T performed in the *C*2/*c* space group, determined by an accurate re-evaluation of the X-ray structure. Positive spin populations were observed on the two manganese sites, and negative spin populations were observed on the molybdenum site, which provides evidence of antiferromagnetic Mo^{3+}–Mn^{2+} exchange interactions through the cyano bridge. The experimental data have been compared to the results of DFT calculations. Moreover, theoretical studies reveal the predominance of the spin polarization mechanism in the Mo–C–N–Mn sequence, with the antiferromagnetic nature of the interaction being due to the overlap between the magnetic orbitals relative to manganese and molybdenum in the cyano bridging region. The magnetic structure of $K_2[Mn(H_2O)_2]_3[Mo(CN)_7]_2 \cdot 6H_2O$ has been solved at low temperature in zero field by powder neutron diffraction measurements. The structure was found to be ferrimagnetic where the manganese and molybdenum spins are aligned along the $\vec{b}$ axis in opposite directions.

1. Introduction

The synthesis and study of cyano-bridged molecule-based magnets has attracted a great deal of attention in the past 20 years.[1] Among them, a family of cyano-bridged compounds based on the $[Mo(CN)_7]^{4-}$ building block is of particular interest because of their original structural organizations and unusual magnetic properties. To date, the synthesis, crystal structures, and magnetic studies of $Mn_2(H_2O)_5[Mo(CN)_7] \cdot nH_2O$ ($n = 4$ and 4.75),[2,3] $(NH_4)_2[Mn(H_2O)_{2.5}]_3[Mo(CN)_7]_2 \cdot 4H_2O$,[4] $Mn_2(tea)[Mo(CN)_7] \cdot nH_2O$ ($n = 0$ or 1; tea = triethanolamine),[5] $[(N(CH_3)_4]_2[Mn(H_2O)]_3[Mo(CN)_7]_2 \cdot 2H_2O$,[6] and $K_2[Mn(H_2O)_2]_3[Mo(CN)_7]_2 \cdot 6H_2O$[7] have been reported.

* To whom correspondence should be addressed. E-mail: gillon@llb.saclay.cea.fr (B.G.); joulia@univ-montp2.fr (J.L.); ruiz@qi.ub.es (E.R.). Fax: (33) 4 67 14 38 52 (B.G.).

† Centre d'Etudes de Saclay.

‡ Université Montpellier II.

§ Universitat de Barcelona.

£ Current address : Institut de Chimie de la Matière Condensée de Bordeaux (ICMCB) (CNRS UPR 9048) 87 av. du Dr. A. Schweitzer 33608 Pessac Cedex, France.

|| Current address : School of Chemistry, University of New South Wales, Sydney NSW 2052, Australia.

(1) (a) Hatlevik, O.; Buschmann, W. E.; Zhang, J.; Manson, J. L.; Miller, J. S. *Adv. Mater.* **1999**, *11*, 914. (b) Holmes, S. M.; Girolami, G. S. *J. Am. Chem. Soc.* **1999**, *121*, 5593. (c) Morin, B. G.; Hahm, C.; Epstein, A. J.; Miller, J. S. *J. Appl. Phys.* **1994**, *75*, 5782. (d) Miller, J. S. *Adv. Mater.* **1994**, *6*, 322. (e) Ferlay, S.; Mallah, T.; Ouahès, R.; Veillet, P.; Verdaguer, M. *Inorg. Chem.* **1999**, *38*, 229. (f) Buschmann, W. E.; Paulson, S. C.; Wynn, C. M.; Girtu, M.; Epstein, A. J.; White, H. S.; Miller, J. S. *Adv. Mater.* **1997**, *9*, 645. (g) Entley, W. R.; Girolami, G. S. *Science* **1995**, *268*, 397. (h) Ferlay, S.; Mallah, T.; Ouahès, R.; Veillet, P. M.; Verdaguer *Nature* **1995**, *378*, 701. (i) Gadet, V.; Mallah, T.; Castro, I.; Verdaguer, M. *J. Am. Chem. Soc.* **1992**, *114*, 9213. (j) Mallah, T.; Thiébaut, S.; Verdaguer, M.; Veillet, P. *Science* **1993**, *262*, 1554. (k) Sato, O.; Iyoda, T.; Fujishima, A.; Hashimoto, K. *Science* **1996**, *271*, 49. (l) Ohkoshi, S.; Hashimoto, K. *J. Am. Chem. Soc.* **1999**, *121*, 10591. (m) Sra, A. K.; Andruh, M.; Kahn, O.; Golhen, S.; Ouahab, L.; Yakhmi, J. V. *Angew. Chem., Int. Ed.* **1999**, *38*, 2606. (n) Zhong, Z. J.; Seino, H.; Mizobe, Y.; Hidai, M.; Fujishima, A.; Ohkoshi, S.-I.; Hashimoto, K. *J. Am. Chem. Soc.* **2000**, *122*, 2952.

10.1021/ic0611645 CCC: $37.00
Published on Web 01/18/2007

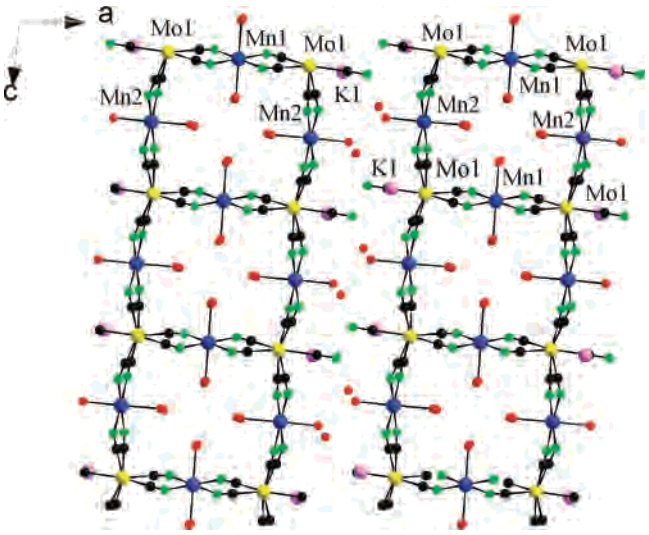

Figure 1. View of the crystal structure of $K_2[Mn(H_2O)_2]_3[Mo(CN)_7]_2 \cdot 6H_2O$ in the $(\vec{a},\vec{c})$ plane. Hydrogen atoms are omitted for clarity.

The last compound has a two-dimensional structure, which may be described as anionic double sheets alternated with the K^+ counterions (Figure 1 and Figures 1S, 2S, Supporting Information).[8,13] The initial magnetic studies performed on the single crystals of this compound found that the predominant magnetic interactions along with $Mn^{2+}-Mo^{3+}$ interactions through the cyano bridge are ferromagnetic.[7] However, the preliminary results of the polarized neutron diffraction on a single crystal[8] and the repeated magnetic measurements[9] established the presence of antiferromagnetic $Mo^{3+}-Mn^{2+}$ interactions. This controversy prompted further investigation of the magnetic properties of this compound in an attempt to shed some light into the exchange mechanism and the magnetic structure.

Neutron diffraction has proven to be a powerful technique for the study of magnetic and structural properties of molecule-based magnets. Neutron powder diffraction data can be used to provide information on the crystal symmetries of compounds, and their structural transitions under different conditions (varying temperature and pressure) permit the determination of magnetic structures and their evolution in function of temperature.[10] The polarized neutron diffraction technique performed on single crystals of magnets offer information on the centers involved in the magnetic coupling and in the mechanism of the coupling itself.[11,12] The method permits the complete determination of the induced spin density distribution for compounds in the solid state. The information obtained from combined neutron diffraction measurements is invaluable to understand the ground state of the magnet, magnetic structures, and the different mechanisms responsible for the magnetic properties.

In this context, we therefore undertook neutron diffraction studies on powder and on single crystals of $K_2[Mn(H_2O)_2]_3[Mo(CN)_7]_2 \cdot 6H_2O$ in order to offer an unambiguous experimental evidence of the exact nature of the magnetic interactions and to determine the magnetic structure of this compound. We also performed a theoretical computational study based on Density Functional Theory for di- and trinuclear models to estimate the exchange coupling constants in the cyano-bridged $Mn^{2+}-Mo^{3+}$ compounds, in order to corroborate the experimental results.

2. Experimental Section

Single-crystal samples of $K_2[Mn(H_2O)_2]_3[Mo(CN)_7]_2 \cdot 6H_2O$ were prepared as previously described.[7] Magnetic susceptibility data were collected on the powder of $K_2[Mn(H_2O)_2]_3[Mo(CN)_7]_2 \cdot 6H_2O$ with a Quantum Design MPMS-XL SQUID magnetometer. The data were corrected for the sample holder, and the diamagnetism contributions calculated from Pascal's constants.[13]

Powder Neutron Diffraction Experiments. Neutron powder diffraction experiments were performed on the two-axis G4.1 diffractometer ($\lambda = 2.4266$ Å) installed at the Orphée reactor in the Laboratoire Léon Brillouin (Saclay, France). The diffraction patterns were collected at several temperatures between 1.4 and 50 K for the determination of the magnetic structure.[14] The experimental neutron diffraction data were analyzed by the Rietveld profile fitting method using the FULLPROF program,[15] based on the nuclear scattering lengths published by Sears.[16]

Neutron Diffraction Measurements on a Single Crystal. Neutron diffraction measurements at 50 K were previously collected at the Laboratoire Léon Brillouin (Saclay, France)[8] in order to provide the hydrogen atom positions and low-temperature structure parameters. However, this data collection was performed assuming

(2) Larionova, J.; Kahn, O.; Gohlen, S.; Ouahab, L.; Clérac, R. *Inorg. Chem.* **1999**, *38*, 3621.
(3) (a) Larionova, J.; Clérac, R.; Sanchiz, J.; Kahn, O.; Gohlen, S.; Ouahab, L. *J. Am. Chem. Soc.* **1998**, *120*, 13088. (b) Larionova, J.; Kahn, O.; Bartolome, J.; Burriel, R.; Castro, M.; Ksenofontov, V.; Gütlich, Ph. *Chem. Mater.* **1999**, *11*, 3400.
(4) Le Goff, X. F.; Willemin, S.; Coulon, C.; Larionova, J.; Donnadieu, B.; Clerac, R. *Inorg. Chem.* **2004**, *43*, 4784−4786.
(5) Tanase, S.; Tuna, F.; Guionneau, Ph.; Maris, T.; Rombaut, G.; Mathoniere, C.; Andruh, M.; Kahn, O.; Sutter, J.-P. *Inorg. Chem.* **2003**, *42*, 1625−1631.
(6) Larionova, J.; Clérac, R.; Donnadieu, B.; Guérin, Ch. *Chem. Eur. J.* **2002**, *8*, 2712−2716.
(7) Larionova, J.; Kahn, O.; Gohlen, S.; Ouahab, L.; Clérac, R. *J. Am. Chem. Soc.* **1999**, *121*, 3349.
(8) Stride, J. A.; Gillon, B.; Gukasov, A.; Larionova, J.; Clérac, R.; Kahn, O. *C. R. Acad. Sci. Paris* **2001**, *4*, 105−112.
(9) Le Goff, X. F.; Clerac, R.; Coulon, C.; Donnadieu, B. *J. Phys. IV* **2004**, 633.
(10) Manson, J. L.; Huang, Q.-Z.; Lynn, J. W.; Koo, H.-J.; Wangbo, M.-H., Bateman, R.; Otsuka, T.; Wada, N.; Argyriou, D. N.; Miller, J. S. *J. Am. Chem. Soc.* **2001**, *123*, 162.
(11) (a) Gillon, B.; Cavata, C.; Schweiss, P.; Journaux, Y.; Kahn, O.; Schneider, D. *J. Am. Chem. Soc.* **1989**, *111*, 7124. (b) Baron, V.; gillon, B.; Plantevin, O.; Cousson, A.; mathonière, C.; Kahn, O.; Grand, A.; Öhrström, L.; Delley, B. *J. Am. Chem. Soc.* **1996**, *118*, 11822. (c) Baron, V.; gillon, B.; Cousson, A.; Mathonière, C.; Kahn, O.; Grand, A.; Öhrström, L.; Delley, B.; Bonnet, M.; Boucherle, J. X. *J. Am. Chem. Soc.* **1997**, *119*, 3500. (d) Aebersold, M.; Gillon, B.; Plantevin, O.; Pardi, L.; Kahn, O.; Bergerat, P., von Seggern, I.; Tuczek, F.; Öhrström, L.; Grand, A.; Lelièvre-Berna, E. *J. Am. Chem. Soc.* **1998**, *120*, 5238. (e) Gillon, B.; Mathonière, C.; Ruiz, E.; Alvarez, S.; Cousson, A.; Rajendiran, T. M.; Kahn, O. *J. Am. Chem. Soc.* **2002**, *124*, 14433.
(12) (a) Zheludev, A.; Bonnet, M.; Ressouche, E.; Schweizer, J.; Wan, M.; Wang, H. *J. Magn. Magn. Mater.* **1994**, *135*, 147. (b) Zheludev, A.; Chiarelli, R.; Delley, B.; Gillon, B.; Rassat, A.; Ressouche, E.; Schweizer, J. *J. Magn. Magn. Mater.* **1995**, *140*, 1439.
(13) Boudreaux, E. A.; Mulay, L. N. *Theory and Applications of Molecular Paramagnetism*; John Wiley Sons: New York, 1976.
(14) Roisnel, T.; Rodriguez-Carjaval, J.; Pinot, M.; André, G.; Bourée, F. *Mater. Sci. Forum* **1994**, *245*, 166.
(15) Rodriguez-Carjaval, J.; Roisnel, T. *IUCr Commission on Powder Diffraction of the XV Congress of the IUCr*; IUCr: Toulouse, France 1991; p 127.
(16) Sears, V. F. *Neutron News* **1992**, *3*, 26.

Table 1. Summary of the Nuclear Structure Refinement of the X-ray and Neutron Diffraction Data

Crystallographic Data from X-ray	
chemical formula	$K_2[Mn(H_2O)_2]_3[Mo(CN)_7]_2 \cdot 6H_2O$
M_r	1015.37
space group	$C2/c$ (No. 15)
cell params (193 K)	$a = 30.911(4)$ Å, $b = 7.188(1)$ Å, $c = 16.208(2)$ Å
	$\alpha = 90.0°$, $\beta = 96.092(2)°$, $\gamma = 90.0°$
V	3580.9(8) Å^3
ρ	1.883 g cm^{-3}
cryst packing	$Z = 4$
no. of atoms in asymmetric unit	36
X-ray Data Collection	
λ	0.71073
T, °C	193 (2)
reflns collected	9812
unique reflns	2554
Structural Refinement Conditions (X-ray)	
refinement method	full-matrix last-squares on F^2
data/restraints/params	2554/81/251
final R indices [$I > 2\sigma(I)$]	R1 = 0.0266 and wR2 = 0.0523
R indices (all data)	R1 = 0.0511 and wR2 = 0.0582
Neutron Data Collection	
diffractometer	4-circle 6T2, LLB, Saclay
monochromator	graphite
neutron wavelength, λ	1.548 Å
T	50 K
measured reflns	686
unique reflns	628
Structural Refinement Conditions (Neutrons)	
unique reflns ($F_N^2 > 3\sigma(F_N^2)$)	372
params	138
R factors	$R(F) = 0.172$ and $R_w(F^2) = 0.190$

[a] $R = \sum |F_o| - |F_c| / \sum |F_o|$. $R_w = \{(\sum_i w_{(i)} [F_{o^2(i)} - F_{c^2(i)}][F_{o^2(i)} - F_{c^2(i)}]) / (\sum_i w_{(i)}[F_{o^2(i)} - F_{o^2(i)}])\}^{1/2}$.

the previously assigned noncentric $C2$ space group,[7] with cell parameters $a = 30.772(12)$ Å, $b = 7.1717(11)$ Å, $c = 8.0738(5)$ Å, and $\beta = 96.006(11)°$. The presence of an inversion center in the $C2/c$ space group results in a doubling of the c cell parameter $a = 30.911(4)$ Å, $b = 7.188(1)$ Å, $c = 16.208(2)$ Å, and $\beta = 96.092(2)°$ (at 193 K).[9,17] The new indexing of the (h, k, l) reflections leads to (h, k, 2l) reflections, and therefore, only reflections with even l values were actually recorded. New refinements of the nuclear structure were carried out in the $C2/c$ space group, on the basis of 388 unique (h, k, 2l) reflections, with $F_N^2 > 2\sigma(F_N^2)$, corrected for absorption. The X-ray structural positions at 193 K were used as starting parameters. Constraints were applied on selected bond lengths Mo−C, Mn−N, Mn−O, C−N, and O−H and angles ∠OMnO, ∠CMoC, ∠NMnO, ∠NCMo, ∠CNMn, ∠MnOH, and ∠HOH for the refinement of the nuclear structure in the $C2/c$ space group (d(O−H)= 0.95(5) Å and ∠HOH = 109.0(3)°). The atomic position and isotropical thermal parameters were refined on F_N^2 using the CRYSTALS program[18] with the same B_{iso} for the two H atoms of each H_2O. Table 1 reports the crystallographic data, along with the experimental conditions.

Unfortunately, it was not possible to get a good refinement of the crystal structure at 50 K due to the fact that all (h, k, 2l + 1)-type reflections were missing in the neutron data collection. This accounts for the poor value of the agreement factor ($R_w(F^2) = 0.22$). However, the high quality of the X-ray structure at 193 K, including the hydrogen positions, to which the structural neutron refinement at 50 K has been closely constrained, justifies the use of the structure at 50 K to calculate the nuclear structure factors for the polarized neutron data treatment.

Table 2. Polarized Neutron Diffraction Data

chemical formula	$K_2[Mn(H_2O)_2]_3[Mo(CN)_7]_2 \cdot 6H_2O$
space group	$C2$ (No. 5)
diffractometer	5C1, LLB, Saclay
polarizing monochromator	Heusler
polarization	0.90
neutron wavelength, λ	0.84 Å
T	4 K
applied magnetic field H	3 T
angle between $\vec{H}$ and $\vec{b}$ (easy axis)	22.2° in the ($\vec{b}$,$\vec{c}$*) plane
measured reflns	216
unique reflns	42

Polarized Neutron Diffraction Data. Experimental procedures and methods for polarized neutron diffraction have been previously described.[19] The experimental quantities that are measured in this technique are the flipping ratios for a set of Bragg reflections of scattering vector, $\vec{K}$, i.e., the ratio $R(\vec{K})$ between the intensities diffracted for an incident neutron beam polarization along the up or down vertical direction, respectively.

$$R(\vec{K}) = \left|\frac{F_N + F_M}{F_N - F_N}\right|^2 \quad (1)$$

A set of flipping ratios was previously collected on the polarized neutron diffractometer 5C1, at the LLB in Saclay (see Table 2). The orientation of the crystal with respect to the vertical magnetic field was such that the easy magnetization axis, $\vec{b}$, was inclined by an angle of 22° toward $\vec{c}$ in the ($\vec{b}$,$\vec{c}$) plane (the hard axis, $\vec{a}$*, being horizontal).

This data collection however was performed assuming a $C2$ space group,[7] and therefore, only (h, k, 2l)-type reflections were recorded. A new refinement of these data has been performed in the centrosymmetric $C2/c$ space group.[9,17] Only reflections for which the flipping ratio was in the range $0.45 < R < 2.2$ have been considered.

Computational Methodology. For the calculation of the coupling constant J for a dinuclear complex, two DFT calculations must be carried out, one for the highest spin state and another one for a low-spin state corresponding to the situation in which both spins are in opposite directions. The J value is obtained using the following equation,

$$E_{HS} - E_{LS} = -(2S_1S_2 + S_2)J \quad (2)$$

where S_1 and S_2 are the total spins of the paramagnetic centers and $S_1 > S_2$ has been assumed for heterodinuclear complexes.[20] In the case of the system under study, we have isolated dinuclear units from the periodic structure consisting of one Mo(III) and one Mn(II) cation. A similar approach can be followed, in general, for any polynuclear complexes with n different exchange constants where the energy of $n + 1$ spin configurations must be calculated.[21] A detailed description of the procedure employed to calculate the

(17) Larionova, J.; Willemin, S.; Donnadieu, B.; Henner. B.; Guérin, C.; Gillon, B.; Goujon, A. *J. Phys. Chem. Sol.* **2004**, *65*, 677−691.
(18) Watkin, D. J.; Prout, C. K.; Carruthers, J. R.; Betteridge, P. W. *Copper, CRYSTALS Issue 11*; Chemical Crystallography Laboratory, University of Oxford: Oxford.
(19) Schweizer, J. *MagnetoScience − From Molecules to Materials*; Miller, J., Drillon, M, Eds.; Wiley: New York, 2001; p 325.
(20) (a) Ruiz, E.; Cano, J.; Alvarez, S.; Alemany, P. *J. Comp. Chem.* **1999**, *20*, 1391. (b) Ruiz, E.; Alvarez, S.; Cano, J.; Polo, V. *J. Chem. Phys.* **2005**, *123*, 164110.
(21) Ruiz, E.; Rodríguez-Fortea, A.; Cano, J.; Alvarez, S.; Alemany, P. *J. Comp. Chem.* **2003**, *24*, 982.

exchange coupling constants in dinuclear and polynuclear complexes can be found in refs 20 and 21.

The hybrid B3LYP functional[22−24] has been used in all calculations as implemented in Gaussian 98.[25] This functional provides excellent results for the calculation of the exchange coupling in a wide range of transition metal complexes.[26−29] We had also found that, when using DFT-based wavefunctions,[30] a reasonable estimate of the low-spin state energy can be obtained directly from the energy of an unrestricted single-determinant solution. This fact is due to the inclusion of the nondynamic correlation effects in the commonly used exchange functionals through the self-interaction error. If spin projection is applied in addition, a cancellation of such correlation effects ensues, as discussed recently by Polo et al.[31] In a previous work, we have found that the use of pseudopotentials is a good approach for the estimation of the exchange coupling for complexes containing second transition series elements.[32] We employed Stoll−Preuss quasi-relativistic pseudopotentials[33] combined with the triple-ζ all-electron basis set for manganese atoms[34] and a double-ζ all-electron basis set for the other elements proposed by Ahlrichs et al.[35]

3. Results

3.1. Magnetic Structure from Neutron Powder Diffraction Measurements. Neutron powder diffraction measurements of the compound $K_2[Mn(H_2O)_2]_3[Mo(CN)_7]_2 \cdot 6H_2O$ were performed in the magnetically ordered domain and in the paramagnetic zone on the G4.1 multidetector. The critical temperature for this compound was found to be 39 K from magnetic susceptibility measurements.[7] In this respect, a series of powder patterns were collected, at 1.4, 10, 20, 30, 40, and 50 K. Two limiting powder patterns are shown in Figure 2, in both the magnetically ordered domain at $T = 1.4$ K and in the paramagnetic domain at $T = 50$ K.

We initially verified that the nuclear structure (space group *C*2/*c*, atomic positions including hydrogens) determined from X-ray data of a single crystal at 193 K gave a qualitatively good refinement of the neutron powder diagram at 50 K. The neutron refinement at 50 K provides the following cell parameters: $a = 30.824(2)$ Å, $b = 7.180(1)$ Å, $c = 16.150(2)$ Å, $\beta = 96.126(6)°$, which are in good agreement with the values obtained by X-ray diffraction (Table 1). Nevertheless, it should be noted that the important number of hydrogen atoms in the structure gives rise to a non-negligible incoherent scattering, visible as the high level of the background of the diffraction patterns.

The appearance of additional contributions of magnetic origin becomes visible at the nuclear Bragg peak positions of the diffraction patterns (characteristic of a ferro- or ferrimagnetic structure) with *n* magnetically ordered domains below 40 K (Figure 2a). The thermal evolution of the observed integrated intensity on the Bragg peak positions present at 24° in 2Θ (3,1,0 and −4,2,0 indices) (Figure 3S, Supporting Information) confirms the presence of the magnetic ordering transition at 39 K.

For the determination of the magnetic structure, several ferromagnetic and ferrimagnetic models were tested within the FULLPROF refinement program, with various relative orientations of the ordered magnetic moments on the three different magnetic atoms of the structure, i.e., Mo atoms in an 8f site, Mn atoms (Mn1 site) in a 4a site and Mn atoms (Mn2 site) in an 8f site. Due to the relatively low percentage of the magnetic atoms in the structure, the magnetic signals are quite small, and as the background of the neutron diagrams is quite high, these magnetic refinements were performed on the difference patterns, $T = 1.4-50$ K.

The magnetic model which gave the best agreement factor in the refinement was obtained for a ferrimagnetic structure where all of the magnetic moments on Mo, Mn1, and Mn2 sites are oriented along the $\vec{b}$ direction with the following values (at 1.4 K): $M_{Mo} = -0.8(2)\ \mu_B$, $M_{Mn1} = 5.0(2)\ \mu_B$, $M_{Mn2} = 4.7(2)\ \mu_B$. This model corresponds to the continuous line in Figure 2b, superimposed on the observed difference diagram 1.4−50 K. It should be noted that the relatively poor value, 24% of the Bragg magnetic agreement factor, is directly linked to the high level of the incoherent scattering due to the hydrogen atoms and the relatively small size of the magnetic signal. The corresponding model magnetic structure is shown in Figure 3.

3.2. Experimental Spin Density from Polarized Neutron Diffraction. The magnetization density $\rho(\vec{r})$ is related to the magnetic structure factor with scattering vector $\vec{K}$ through a Fourier transformation:

$$F_M(\vec{K}) = \int_{cell} \rho(\vec{r})\, e^{i\vec{K}\vec{r}}\, d\vec{r} \qquad (3)$$

The experimental magnetic structure factors F_M^{exp} for the set of measured Bragg reflections are directly deduced from the flipping ratios using eq 1, knowing F_N. Therefore the precision obtained on F_M^{exp} depends also on the quality of the structure determination.

(22) Becke, A. D. *J. Chem. Phys.* **1993**, *98*, 5648.
(23) Becke, A. D. *Phys. Rev. A* **1988**, *38*, 3098.
(24) Lee, C.; Yang, W.; Parr, R. G. *Phys. Rev. B* **1988**, *37*, 785.
(25) Frisch, M. J.; Trucks, G. W.; Schlegel, H. B.; Scuseria, G. E.; Robb, M. A.; Cheeseman, J. R.; Zakrzewski, V. G.; Montgomery, J. A., Jr.; Stratmann, R. E.; Burant, J. C.; Dapprich, S.; Millam, J. M.; Daniels, A. D.; Kudin, K. N.; Strain, M. C.; Farkas, O.; Tomasi, J.; Barone, V.; Cossi, M.; Cammi, R.; Mennucci, B.; Pomelli, C.; Adamo, C.; Clifford, S.; Ochterski, J.; Petersson, G. A.; Ayala, P. Y.; Cui, Q.; Morokuma, K.; Malick, D. K.; Rabuck, A. D.; Raghavachari, K.; Foresman, J. B.; Cioslowski, J.; Ortiz, J. V.; Stefanov, B. B.; Liu, G.; Liashenko, A.; Piskorz, P.; Komaromi, I.; Gomperts, R.; Martin, R. L.; Fox, D. J.; Keith, T.; Al-Laham, M. A.; Peng, C. Y.; Nanayakkara, A.; Gonzalez, C.; Challacombe, M.; Gill, P. M. W.; Johnson, B. G.; Chen, W.; Wong, M. W.; Andres, J. L.; Head-Gordon, M.; Replogle, E. S.; Pople, J. A. *Gaussian 98*, revision A.11; Gaussian, Inc.: Pittsburgh, PA, 1998.
(26) Ruiz, E.; Alemany, P.; Alvarez, S.; Cano, J. *J. Am. Chem. Soc.* **1997**, *119*, 1297.
(27) Ruiz, E.; Alvarez, S.; Rodríguez-Fortea, A.; Alemany, P.; Pouillon, Y.; Massobrio, C. Electronic Structure and Magnetic Behavior in Polynuclear Transition-metal Compounds. In *Magnetism: Molecules to Materials*; Miller, J. S., Drillon, M., Eds.; Wiley-VCH: Weinheim, 2001; Vol. 2, p 227.
(28) Ruiz, E.; Cano, J.; Alvarez, S.; Alemany, P. *J. Am. Chem. Soc.* **1998**, *120*, 11122.
(29) Desplanches, C.; Ruiz, E.; Rodríguez-Fortea, A.; Alvarez, S. *J. Am. Chem. Soc.* **2002**, *124*, 5197.
(30) Koch, W.; Holthausen, M. C. A *Chemist's Guide to Density Functional Theory*; Wiley-VCH Verlag: Weinheim, 2000.
(31) Polo, V.; Kraka, E.; Cremer, D. *Theor. Chem. Acc.* **2002**, *107*, 291.
(32) Desplanches, C.; Ruiz, E.; Alvarez, S. *Eur. J. Inorg. Chem.* **2003**, *9*, 1756.
(33) Andrae, D.; Haeussermann, U.; Dolg, M.; Stoll, H.; Preuss, H. *Theor. Chim. Acta* **1990**, *77*, 123.
(34) Schaefer, A.; Huber, C.; Ahlrichs, R. *J. Chem. Phys.* **1994**, *100*, 5829.
(35) Schaefer, A.; Horn, H.; Ahlrichs, R. *J. Chem. Phys.* **1992**, *97*, 2571.

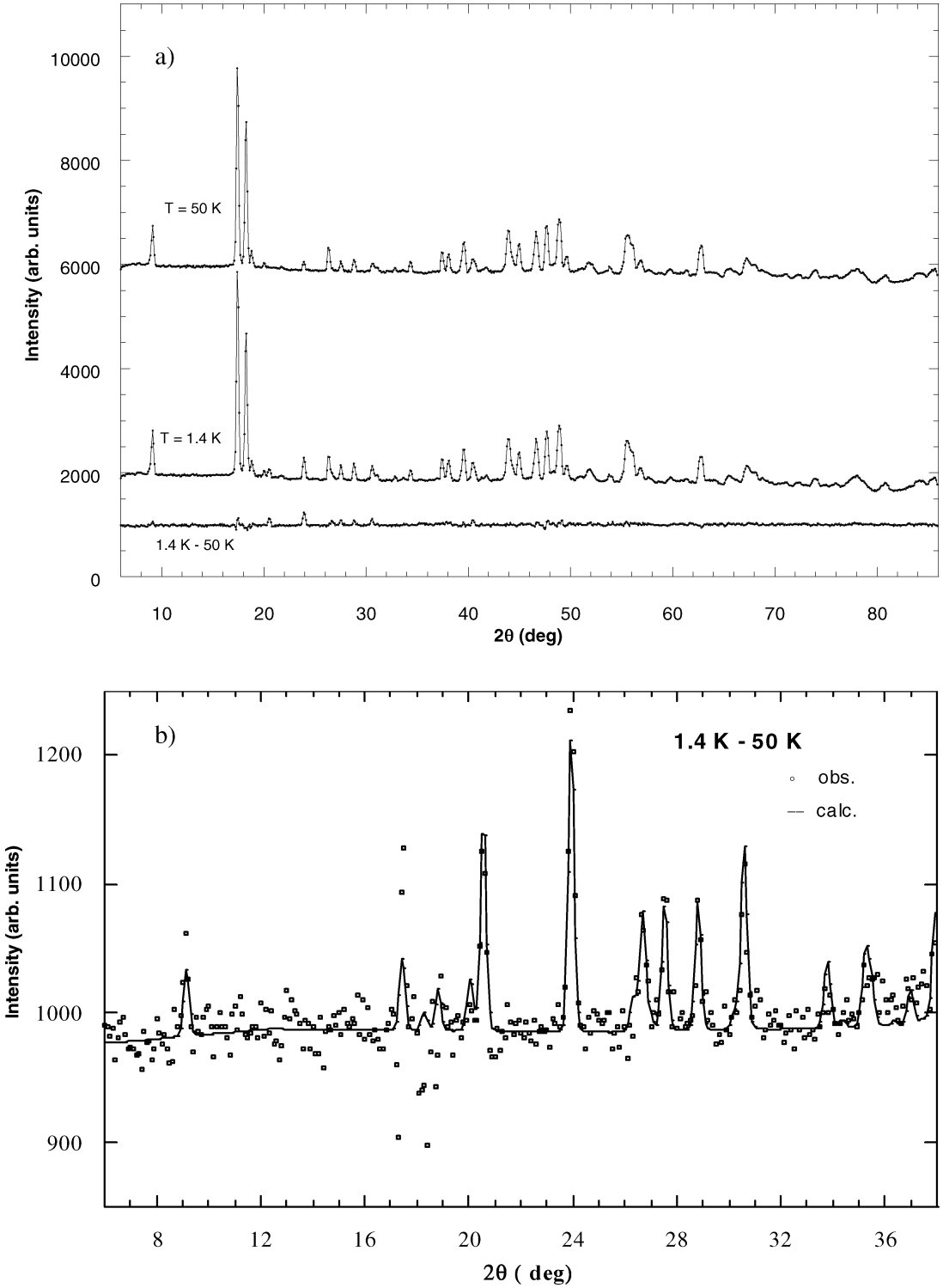

Figure 2. (a) Neutron diffraction powder patterns in the magnetically ordered state at 1.4 K and in the paramagnetic state at 50 K for $K_2[Mn(H_2O)_2]_3[Mo(CN)_7]_2 \cdot 6H_2O$. (b) Difference pattern 1.4−50 K. Black dots, experimental points; continuous line, ferrimagnetic model.

The measurements were performed in the magnetically ordered state (under saturated magnetization) at 4 K using an applied magnetic field of 3 T in order to maximize the intensity of the signal. The magnetic field was applied along the crystallographic $\vec{b}$ axis, which also is the magnetic axis. The magnetic structure factors, F_M, were deduced from the experimental flipping ratios with the help of the low-temperature nuclear structure factors calculated from the nuclear structure performed at 50 K. A set of 41 magnetic structure factors for (h, k, 2l) unique reflections, with $F_M > \sigma(F_M)$, was obtained. The measured F_M values were corrected for the contribution arising from the nuclear polarization of the hydrogen nuclear spins. In the experimental conditions of temperature and field, the calculated value for the hydrogen nuclear spin polarization f^{H}_{NP} is equal to 0.00372 $\times 10^{-12}$ cm.

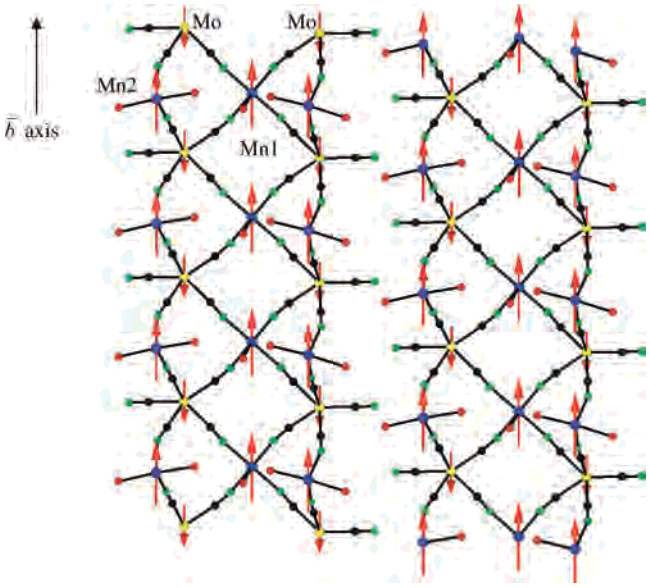

Figure 3. Magnetic structure model determined for $K_2[Mn(H_2O)_2]_3[Mo(CN)_7]_2 \cdot 6H_2O$.

The analysis of the polarized neutron diffraction data consists in refining a multipole model of the spin density $\rho(\vec{r})$ by a least-squares procedure on the basis of the magnetic structure factors, F_M.[36] It should be noted that the accurate determination of the crystal structure of $K_2[Mn(H_2O)_2]_3[Mo(CN)_7]_2 \cdot 6H_2O$ shows that the compound crystallizes in monoclinic centrosymmetrical $C2/c$ (No.15) space group. Consequently, a direct determination of the magnetic structure factor using this approach should be available. In the model used, the spin density $\rho(\boldsymbol{r})$ is written as a sum of atomic spin densities $\rho_i(\vec{r}_i)$ centered on the atoms i:

$$\rho_i(\vec{r}_i) = \sum_{l=0}^{4} R_l^i(\kappa_i r_i) \sum_{m=-1}^{1} P_{lm}^i y_{lm}^i(\theta_i, \varphi_i) \qquad (4)$$

where P_{lm}^i are the multipole populations, $R_l^i(\kappa_i r_i)$ is a Slater-type radial function $R_l^i(\kappa r) = N_R r^{n_1} e^{-\kappa\zeta r}$ and y_{lm}^i is a real spherical harmonics. The radial exponents ζ were taken from the literature:[37] $n = 4$, $\zeta_{Mn} = 7.02$ for Mn^{2+} ($3d^5$), $n = 6$, $\zeta_{Mo} = 6.21$ for Mo^{3+} ($4d^5$), and $n = 2$, $\zeta_N = 3.84$, $\zeta_C = 3.14$ for N and C. A spherical model including monopoles on Mn1, Mn2, and Mo was applied. The radial contraction coefficients, κ_i, have been refined only for the Mn and Mo atoms. The populations of the N atoms (and respectively for the C atoms) belonging to the plane were constrained to be equal, and on the other hand, the N and C populations of the bridges between the planes were constrained to have the same values as the N and C atoms of the plane, respectively.

The results of the multipole refinements are reported in Table 3. A first series of refinements were performed on the set of 41 experimental magnetic structure factors. The opposite signs of the spin populations on the manganese and molybdenum atoms confirm the antiferromagnetic nature of the $Mn^{2+}-Mo^{3+}$ interactions, which was first suggested in the previous polarized neutron data analysis.[8] No significant populations were obtained either on the nitrogen or on the carbon atoms. The magnitude of the populations of the manganese and the molybdenum ions is much weaker than the values 5 μ_B and 1 μ_B expected for $S_{Mn} = 5/2$ and $S_{Mo} = 1/2$ local spins at magnetic saturation. The total induced moment on the $\{Mn_3Mo_2\}$ unit derived from the refinement given by the sum of the spin populations is 10.75(4) μ_B, which is lower than the expected value of 12.8 μ_B according to the supplementary SQUID magnetic measurements (Figure 4S, Supporting Information).

Table 3. Atomic Spin Populations in $K_2[Mn(H_2O)_2]_3[Mo(CN)_7]_2 \cdot 6H_2O$[a]

Refinement Conditions		
	without $F_M(0, 0, 0)$	with $F_M(0, 0, 0)$
unique reflns	37	38
params	5	5
GOF (χ)	1.15	1.74
R_w (F_M)	0.07	0.05

Radial κ Coefficients and Spin Populations (in μ_B)		
atom	refinement I	refinement II
κ^{Mo}	0.62 (3)	0.67(6)
κ^{Mn}	0.95 (2)	0.78(2)
Mo	−0.93 (5)	−0.91(6)
Mn1	3.91 (6)	4.83(6)
Mn2	4.23 (4)	4.93(5)
M_{sum}	10.51(11)	12.87(12)

[a] Refined parameters used in modeling the spin density and the refinement statistics. Refinement 1 was carried out without the (0, 0, 0) reflection, and refinement 2 was carried out with the (0, 0, 0) reflection.

In order to correct this incoherence, a second series of multipole refinements were performed (Table 3). In this series, the $F_M(000)$ magnetic structure factor was included, which is equal to $4M$, where M is the measured bulk magnetization value per $\{Mn_3Mo_2\}$ unit in the same temperature and field conditions. Again, the spin populations on the manganese and molybdenum atoms with the opposite sign were observed, and no significant populations were obtained on the nitrogen and carbon atoms. The sum of the populations in the $\{Mn_3Mo_2\}$ unit was found very close to 13 μ_B, and the Mn1, Mn2, and Mo populations are, respectively, equal to 4.83(6), 4.93(5), and −0.91(6) μ_B. The corresponding spin density map projected along the crystallographic $\vec{b}$ axis is shown in Figure 4. The spin population on the molybdenum ion (−0.91(6) μ_B) corresponds to 91% of what is expected for a local spin $S_{Mo} = 1/2$. This finding suggests the spin of the molybdenum ions are not strictly localized on the metal ions but are partially delocalized (around 9%) onto the cyano ligands. The spin populations on the two manganese sites, Mn1 and Mn2, are very close to the value expected for a $S_{Mn} = 5/2$ (97% for Mn1 and 99% for Mn2). Consequently, the delocalization from the manganese ions toward the cyano ligands appears to be weaker than the delocalization observed from the molybdenum ion. This fact is in agreement with the stronger covalent character of the 4d Mo^{3+} ion with respect to the 3d Mn^{2+} ion. As can be seen on the spin density map, the spin density

(36) Brown, P. J.; Capiomont, A.; Gillon, B.; Schweizer, J. *J. Magn. Magn. Mater.* **1979**, *14*, 289.
(37) Clementi, E.; Raimondi, D. L. *J. Chem. Phys.* **1963**, *38*, 2686.

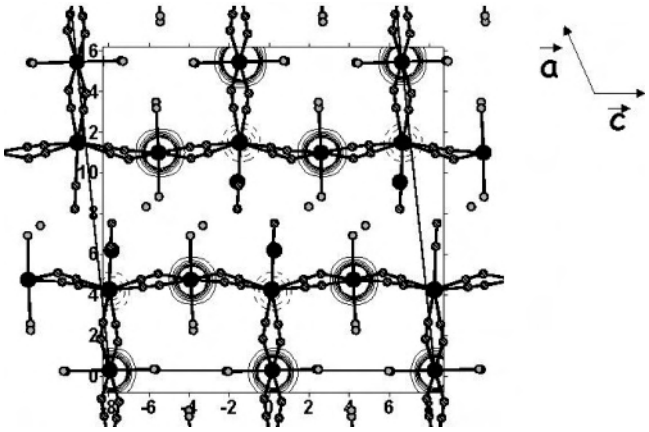

Figure 4. Spin density map of $K_2[Mn(H_2O)_2]_3[Mo(CN)_7]_2 \cdot 6H_2O$ at 4 K and in an applied field of 3 T, projected along the crystallographic $\vec{b}$ axis. High-level contour shows the dominant spin populations of the metal sites (solid lines, positive contours; dashed lines, negative contours. Contours levels: −0.1, −0.08, −0.06, −0.04, −0.02, 0.02, 0.04, 0.06, 0.08, 0.1).

located on molybdenum ions is more diffuse than the density located on the manganese ions, which is in agreement with the larger radial extension of 4d orbitals compared to 3d orbitals.

3.3. Density Functional Theory Results. In this theoretical section, the first part will be devoted to the study the exchange coupling in $K_2[Mn(H_2O)_2]_3[Mo(CN)_7]_2 \cdot 6H_2O$ using di- and trinuclear molecular models. The second part will present the calculation of the atomic spin populations obtained with theoretical approach in order to compare the results with the data obtained by the polarized neutron diffraction measurements.

3.3.1. Theoretical Evaluation of the Exchange Coupling Constant. Due to the low symmetry of the system and the presence of multiple interactions, to carry out the calculation of the exchange coupling constants using a periodic model is computationally very demanding and the presence of the second-neighbor contributions would make the treatment almost impossible. Hence, the calculations of the exchange coupling constant have been carried out employing dinuclear or trinuclear units extracted from the crystal structure including all the cyanide ligands and water molecules coordinated to such metals (Figure 1). The covalent character of the chemical bonding to the cyanide ligands present in the structure ensures that such dinuclear complexes are realistic models of the whole structure. The analysis of the crystal structure indicated the presence of six different exchange coupling pathways through the cyanide ligands between the Mo^{3+} and Mn^{2+} ions (Figure 1). The crystal structure shows planes of Mo^{3+} cation surrounded by four Mn^{2+} cations, with the other two Mn^{2+} cations bridging the planes. The seventh coordination site of the Mo^{3+} cation is occupied by a nonbridging cyanide ligand. Thus, we can classify the exchange couplings pathways in two groups, the first one containing the four different interactions present in the planes (Figure 5) and the other two corresponding to the interaction of the Mo^{3+} cations with the bridging Mn^{2+} centers. The results corresponding to the six exchange coupling constants are collected in Table 4.

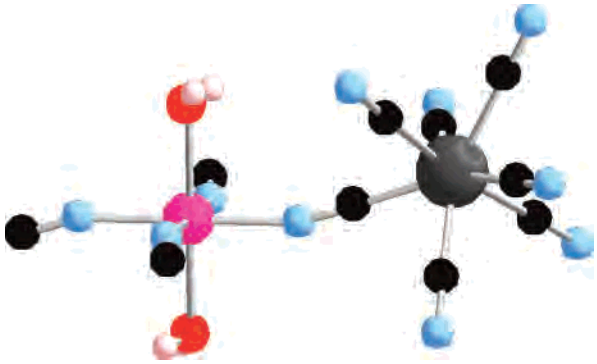

Figure 5. Models used to carry out the calculations of the exchange coupling constant. The dinuclear unit extracted from the crystal structure including all the cyanide ligands and water molecules coordinated to such metals.

Table 4. Calculated Exchange Coupling Constants (in cm^{-1}) Using the B3LYP Functional for Six Dinuclear Models of $[MoMn(CN)_{10}(H_2O)_2]^{5-}$ Corresponding to the Different Exchange Interactions in the Structure of $K_2[Mn(H_2O)_2]_3[Mo(CN)_7]_2 \cdot 6H_2O$[a]

	d(Mo···Mn) (Å)	Mn−N−C (deg)	J (cm^{-1})
bridge 1	5.395	163.1	−9.7
bridge 2	5.377	161.9	−42.4
plane 1	5.439	159.6	−2.7
plane 2	5.471	169.9	−5.3
plane 3	5.395	153.0	−7.6
plane 4	5.462	175.3	−36.9

[a] We have indicated some structural parameters related with the exchange pathways to help their identification, likewise, such parameters are also those relevant to control the strength of the exchange coupling.

These results indicate ferrimagnetism for all interactions between the Mo^{3+} and Mn^{2+} cations; likewise, they confirm those obtained from experimental spin density obtained using polarized neutron diffraction and by the recent measures of the magnetic susceptibility despite the ferromagnetic character reported initially.[7] From the theoretical point of view, an antiferromagnetic coupling can be expected due to the presence of one unpaired electron on each d orbital of the Mn^{2+} cations. The Kahn−Briat model[38−40] in this case suggests that the overlap between such magnetic orbitals with that bearing the unpaired electron of the Mo^{3+} will be non-negligible, resulting in an antiferromagnetic interaction.

The strength of the interaction seems to be related with the angles of the bridging bonds and the bond distances. Indeed, the strongest interactions are observed for *plane4* and *bridge2* which have, respectively, the most linear geometry and the shortest Mo−Mn distance. In order to analyze the presence of ferromagnetic couplings, we have carried out the calculation of the exchange coupling constants for trinuclear complexes to know the sign of the second neighbor interaction. There are many possible ways to choose trinuclear complexes with which to study the second neighbor interactions from the crystal structure. We have selected two different models; in the first case we want to calculate the second neighbor exchange constant between two Mn^{2+} cations (Figure 6a), while the second model allows the calculation of the exchange coupling between the Mo^{3+}

(38) Kahn, O.; Briat, B. *J. Chem. Soc. Trans.* **1976**, *72*, 268.
(39) Kahn, O.; Briat, B. *J. Chem. Soc. Trans.* **1976**, *72*, 1441.
(40) Kahn, O. *Molecular Magnetism*; VCH Publishers: New York, 1993.

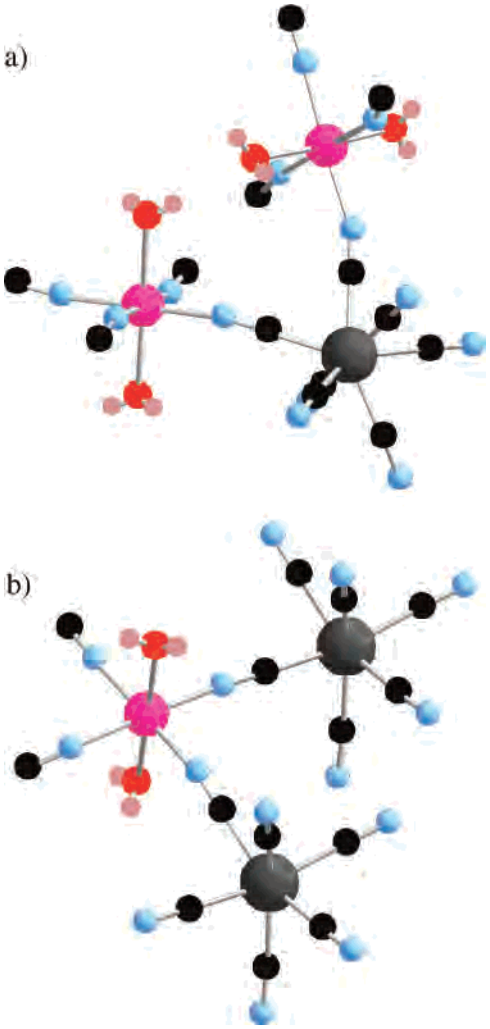

Figure 6. (a) First trinuclear model selected to calculate the second neighbor exchange constant between two Mn(II) cations. (b) The second trinuclear model allows the calculation of the exchange coupling between the Mo(III) cations.

cations (Figure 6b). We have selected these two models because we can expect, due to the angle between the two exchange pathways (close to 90°), that they are good candidates to present ferromagnetic coupling between second neighbors.

The calculated second neighbor exchange coupling between the two Mn^{2+} cations for model **2**, which corresponds to *plane1* and *bridge1* interactions (see Table 4), is -0.26 cm^{-1}. In the model **3** constituted by the *plane1* and *plane2* interactions, the exchange coupling constant corresponding to the interaction between the two Mo^{3+} cations is -1.3 cm^{-1}. From these calculated values, we can conclude that all the second neighbor interactions are probably small and antiferromagnetic.

3.3.2. Spin Density Distribution Study. The second goal of our theoretical study is to analyze the spin density distribution of $K_2[Mn(H_2O)_2]_3[Mo(CN)_7]_2 \cdot 6H_2O$. In order to keep the original coordination of the metals, especially of the Mo^{3+} cation, we have employed a larger molecular model than in the calculations to obtain the exchange coupling constants. The spin population in a model including the six manganese atoms that surround the molybdenum atom is shown in Figure 7.

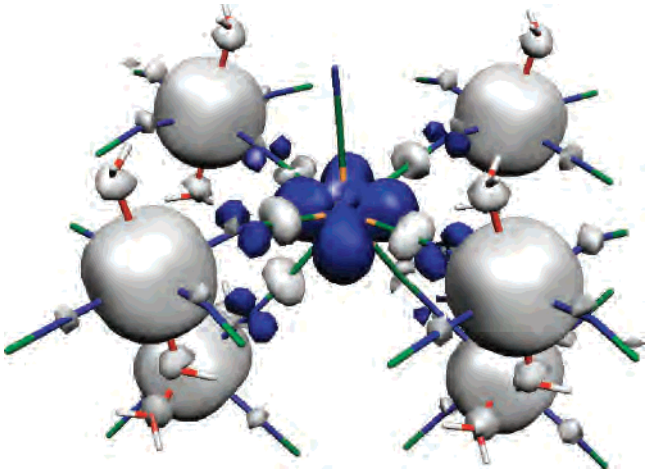

Figure 7. Spin population map corresponding to the $[Mo(CN)_7(Mn(CN)_3(H_2O)_2)_6]^{10-}$ model using the B3LYP method considering the case with antiferromagnetic coupling between the Mn(II) and Mo(III) cations.

Table 5. Calculated Spin Populations Using the B3LYP Functional and the NBO and Mulliken Procedures for the Model $[Mo(CN)_7(Mn(CN)_3(H_2O)_2)_6]^{10-}$ (See Figure 1) and the Available Experimental Data Obtained Using the Polarized Neutron Diffraction (pnd)

atom	NBO	Mulliken	pnd
Mo	−0.81	−0.96	−0.91(6)
Mn	4.75	4.84	4.83(6)
			4.93(5)
N plane	−0.04	−0.07	
C plane	0.06	0.10	
N out of plane	−0.03	−0.05	
C out of plane	0.05	0,10	
N nonbridging	<−0.01	−0.01	
C nonbridging	<0.01	0.01	
O	0.02	<0.01	

The corresponding numerical values of the spin population using NBO[41] and Mulliken procedures are collected in Table 5. The values obtained with both methods are similar but giving for the NBO results a less polarized picture of the spin density in agreement with a previous similar study of a Mn(II)Ni(II) chain complex.[11e] The polarization mechanism is the predominant one in the Mo−C−N−Mn atom sequence.[42] In Figure 9 the spherical shape of the spin population in the manganese ions can be clearly seen. In the case of the molybdenum ion, the shape of the spin density indicates that the d orbital bearing the unpaired electron is almost perpendicular to the direction of the nonbridging cyanide. The nitrogen atoms corresponding to the *plane* and *bridge* interactions have two different contributions, a small one in the σ system, due to delocalization of the manganese ions and a more important one, in the π system, due to the polarization mechanism of the spin density of the molybdenum ion. The spin density on the carbon atoms shows an almost spherical distribution probably due to the low

(41) Reed, A. E.; Curtiss, L. A.; Weinhold, F. *Chem. Rev.* **1988**, *88*, 899.
(42) (a) Cano, J.; Ruiz, E.; Alvarez, S.; Verdaguer, M. *Comments Inorg. Chem.* **1998**, *20*, 27. (b) Ruiz, E.; Cirera, J.; Alvarez, S. *Coord. Chem. Rev.* **2005**, *249*, 2649.

symmetry of the coordination sphere of the molybdenum ions. The delocalization mechanism is the predominant one, in the oxygen atoms of the water molecules and the nitrogen atoms of the terminal cyanide ligands.

We have calculated also the ferromagnetic solution for the $[Mo(CN)_7(Mn(CN)_3(H_2O)_2)_6]^{10-}$ model that will allow the estimation of an average exchange coupling constant for the six-exchange pathway considering the second neighbor interactions to be negligible. The obtained value is -20.1 cm^{-1}; this result is consistent with the values calculated previously with the dinuclear models indicated in Table 4.

4. Discussion

$K_2[Mn(H_2O)_2]_3[Mo(CN)_7]_2\cdot 6H_2O$ is the two-dimensional compound among the family of heptacyanomolybdate molecule-based magnets, in which the structural and magnetic properties have been thoroughly characterized. Previous studies alluded to some controversy concerning about the nature of the $Mn^{2+}-Mo^{3+}$ magnetic interactions through the cyano bridge. Ferromagnetic interactions were found by the primary magnetic measurements performed on the single crystals of $K_2[Mn(H_2O)_2]_3[Mo(CN)_7]_2\cdot 6H_2O$, while antiferromagnetic interactions were established by the neutron diffraction measurements. By combining the different experimental techniques, such as powder neutron diffraction measurements, polarized neutron diffraction on single crystals, repeated magnetic measurements, and theoretical investigations, we attempt here to shed some light on these ambiguous outcomes. (i) First, the magnetic ground state of the $K_2[Mn(H_2O)_2]_3[Mo(CN)_7]_2\cdot 6H_2O$ system was determined by using powder neutron diffraction measurements. The results obtained are in total agreement with a ferrimagnetic structure in which the magnetic moments of manganese atoms (Mn1 and Mn2) and molybdenum atoms are parallel and antiparallel, respectively, to the easy magnetic direction, $\vec{b}$. The sum of the obtained magnetic moments in the magnetic ordered domain at 1.4 K ($(2 \times 4.7) + 5.0 - (2 \times 0.8) = 12.8\ \mu_B$) provides the value of the saturation magnetization 12.8 μ_B. This value corresponds to the calculated value (13 μ_B) for antiferromagnetic $Mn^{2+}-Mo^{3+}$ interactions. (ii) Second, the local spin density map was obtained by polarized neutron diffraction measurements performed on a single crystal at 4 K under a field of 3 T. The spin density at the manganese sites (Mn1 and Mn2) of this material was found to be positive and close to the spin-only values for the free ions. In contrast, the molybdenum sites were found to lie in regions of negative spin density. The opposite signs of the spin densities upon the metals also reflect an antiferromagnetic $Mn^{2+}-Mo^{3+}$ interaction through the cyano bridge. (iii) The repeated SQUID magnetic measurements performed on a powder sample of this compound sealed in a paraffin bag show that the value of the saturation magnetization at 2 K is equal to 12.8 μ_B, characteristic of antiferromagnetic interactions. (iv) Theoretical results using the hybrid B3LYP functional indicate that the exchange interactions between the Mo and Mn ions in $K_2[Mn(H_2O)_2]_3[Mo(CN)_7]_2\cdot 6H_2O$ are antiferromagnetic. In addition, the analysis of the calculated second neighbor exchange coupling between the two Mn^{2+} or the two Mo^{3+} cations, in the considered cases, shows that such values are small and antiferromagnetic. Hence, no ferromagnetic interactions seem to be present in such a compound.

Consequently, the agreement between the ordered magnetic moments values from powder and polarized measurements at magnetic saturation, renewed field dependence magnetization measurements, and theoretical investigations allows us to establish the presence of antiferromagnetic interactions between manganese and molybdenum atoms through the cyano bridge in the $K_2[Mn(H_2O)_2]_3[Mo(CN)_7]_2\cdot 6H_2O$ compound.

Another point to note concerns the agreement between the experimental neutron diffraction spin distribution and the calculated density functional theory results. The main features of the observed spin densities in this two-dimensional compound are satisfactorily reproduced by both NBO and Mulliken calculations on a heptanuclear model including the molybdenum atom surrounded by the six manganese atoms. The observed spin populations on Mn1, Mn2, and Mo atoms are well described by calculations. Nevertheless, small spin population contributions were found by computation on the nitrogen, carbon, and oxygen atoms, while no any population on the ligands was observed in the polarized neutron diffraction spin density map. Apparently, the small populations on the ligands are more sensitive to the refined spin density model than the main spin populations on manganese and molybdenum atoms and the restriction of the neutron data collection limits the quality of refinement. The analysis of the theoretical spin populations reveals the predominance of the polarization mechanism in the Mo−C−N−Mn sequence being the spin density of the Mo ion located in a d orbital almost perpendicular to the nonbridging cyanide ligand.

Finally, a ferrimagnetic structure, in which the magnetic moments on the manganese and on the molybdenum atoms are, respectively, parallel and antiparallel to the easy magnetic $\vec{b}$ axis was obtained from the refinement of powder neutron diffraction measurements. This result is also in agreement with the features obtained from neutron diffraction on the single crystal. On the other hand, due to the small intensity of the magnetic signal and high level of the incoherent scattering due to hydrogen atoms, it cannot be excluded that some canting from the $\vec{b}$ axis of the magnetic moments, especially of the small moment on the molybdenum atom, is present in this compound.

Acknowledgment. The research has been supported by the Direction General de Investigación del Ministerio de Educación y Ciencia and Comissió Interdepartamental de Ciència i Tecnologia (CIRIT) through Grants No. CTQ2005-08123-C02-02/BQU and 2005SGR-00036, respectively. The computing resources were generously made available in the Centre de Computació de Catalunya (CESCA) with a grant provided by Fundació Catalana per a la Recerca (FCR) and the Universitat de Barcelona. C.D. thanks the Program

Improving the Human Research Potential and the Socio-economic Knowledge Base of the European Commission (Contract No. HPMF-CT-2000-00977) for a grant during his postdoctoral stay in Barcelona. J.L., S.W., and Ch.G. thank the University Montpellier 2 and CNRS for financial support. The authors thank Mr. Bruno Donnadieu (LCC, Toulouse, France) for the X-ray structural data and helpful discussion and Dr. Rodolphe Clérac (CRPP, Bordeaux, France) for preliminary magnetic measurements.

Supporting Information Available: Crystal structures, thermal evolution data, and magnetization field dependence data. This material is available free of charge via the Internet at http://pubs.acs.org.

IC0611645